RSC Advances

PAPER

View Article Online
View Journal | View Issue

Cite this: *RSC Adv.*, 2023, **13**, 1333

Exploration of active sites of ethyl alcohol electro-oxidation on porous gold nanoparticles with enhanced Raman spectroscopy†

Yusong Wang,[a] Peng Xu,[b] Wenjie Xie,[a] Shaozhen Wang,[a] Yunyan Chen,[a] Nan Yu[b] and Shengpeng Zhang*[a]

Received 23rd June 2022
Accepted 5th December 2022

DOI: 10.1039/d2ra03863c

rsc.li/rsc-advances

Novel porous gold nanospheres are prepared by calcination of the gold–urea complexes. The enhanced Raman spectra of ethanol catalyzed by different doses of porous gold nanospheres are measured with a 532 nm laser as the excitation source, and an enhanced charge coupled device served in spectral detection and microscopic imaging. The electrochemical experiments show that the catalytic oxidation products of ethanol with porous gold nanoparticles are acetaldehyde, acetic acid, and water, which further proved that the porous gold nanoparticles can activate the $-CH_2$ of ethanol.

1. Introduction

Noble metal catalysts with high catalytic activity and selectivity, as well as high temperature tolerance, chemical stability and other comprehensive excellent properties, in petrochemical, pharmaceutical, pesticide, food, environmental protection, energy, electronics and other fields occupy an extremely important position. With the increasing demands of various industries and decreasing natural resources, we need efficient and environmentally friendly catalytic methods.[1] The suitably prepared gold-based catalyst has strong catalytic activity.[2,3] In the past few decades, Au has been developed as a potential catalyst in a variety of chemical reactions,[4] including selective oxidation,[5–7] selective hydrogenation,[8–10] carbonylation,[11–13] cyclization,[14–16] and three-component coupling reactions.[17–19] The catalytic ability of gold was greatly influenced by microscopic appearance.[20] However, a large number of experiments and studies show that the catalytic ability of noble metal catalysts is not only based on the influence of structure, but also based on the selective binding of related sites with organic compounds.[21]

At present, the detection methods of selective binding between catalysts and organic compounds are TEM, XAS, MS and so on.[22–24] However, there are few studies on the detection of related sites by enhanced Raman spectroscopy. Therefore, it is still meaningful to develop an enhanced Raman spectroscopy method to detect the related catalytic site. Herein, we report that the sites of ethanol catalyzed oxidation by porous Au nanospheres were investigated by enhanced Raman spectroscopy. The porous Au nanospheres are prepared by calcining the complex of chloroauric acid urea. The effects of different doses of porous Au nanospheres were investigated by using anhydrous ethanol enhanced Raman spectrum. After removing the influence of surface plasmon resonance properties of porous Au nanospheres, the actual enhanced Raman spectra of anhydrous ethanol were obtained. The results showed that the optimal dosage of porous Au nanospheres was 0.08 mg mL^{-1} and the catalytic site for ethanol oxidation was $-CH_2$.

2. Experimental

2.1 Materials

$HAuCl_4 \cdot 3H_2O$, 0.05 μm alumina polishing powder, Nafion (5%), potassium ferricyanide, potassium chloride was purchased from Aladdin (Shanghai, China). Urea and ethanol were purchased from Shantou Xilong and Tianjin Fuchen. All aqueous solutions were prepared by deionized water (18.25 MΩ cm).

2.2 Characterizations

Transmission electron microscope (TEM) images were captured using a transmission electron microscope (S-4800, Japan). The Q-switched YAG laser (Indi-10) from American Spectral Physics Corporation was used for laser irradiation. The laser beam was focused using a neutral density filter and a quartz converging lens with a focal length of 100 mm. An imaging lens with a focal length of 70 mm and an optical fiber probe were used to collect the laser signal. The two-dimensional electric translation table was used to move the experimental samples at a precise speed to ensure the sampling quantity and randomness. Sampling

[a]AnHui Provincial Engineering Research Center for Polysaccharide Drugs and Institute of Synthesis and Application of Medical Materials, Department of Pharmacy, Wannan Medical College, Wuhu 241002, P.R. China. E-mail: zhangshengpeng@wnmc.edu.cn
[b]Anhui Normal University, Wuhu 241002, P. R. China

† Electronic supplementary information (ESI) available. See DOI: https://doi.org/10.1039/d2ra03863c

and analysis were performed using grating spectrometer, ICCD and computer. Raman spectroscopy of anhydrous ethanol was detected by self-assembled Raman spectrometer and electrochemical detection of porous Au nanospheres was carried out by electrochemical workstation (CHI660E, Shanghai Chenhua Instrument). Renishaw inVia with a laser wavelength of 532 nm was used for electrochemical enhanced Raman instrument test various substances in the preparation process are dispersed by ultrasonic cleaner.

2.3 Synthesis of porous Au nanospheres

At room temperature, 0.2 g urea was dissolved in 10 mL of deionized water. When completely dissolved, add 1 mL chloroauric acid and stir at 100 °C for 5 min (400 RPM). The prepared mixture was transferred to a dry round-bottom flask with a condensing device and placed in a 100 °C oil bath for reflux for 12 min. After the reaction was completed, the water and alcohol were washed twice, respectively, and dispersed with 1 mL ethanol. Put in the oven at 180 °C for 7 min. The solution turned from yellow to purple after drying and cooling, and then porous gold nanospheres were obtained. Wash with deionized water and ethanol three times respectively, and store for later use.

2.4 Electrochemical catalysis of ethanol

The glassy carbon electrode is used as the working electrode, the saturated calomel as the reference electrode and the platinum wire as the counter electrode. The cyclic voltammetry of the solution was measured at a scanning rate of 150 mV s^{-1} in a potential window of −0.2 to 1.0 V at room temperature. Firstly, the working electrode was polished with a chamois abrasive plate with 0.05 μm Al_2O_3 polishing powder. The polished electrode was placed in a glass bottle with 1 mmol per L potassium ferric cyanide and 0.1 mol per L KCl solution for CV (Cyclic Voltammetry) curve. Only when the potential difference between reduction peak and oxidation peak was less than 80 mV, the working electrode met the use standard. The KOH ethanol solution of 3/4 glassware is added into a clean glassware and sealed, then the glassware is filled with nitrogen for 30 minutes before standby. 0.336 mL H_2O, 0.644 mL DMF, 20 μL Nafion solution and 1 mg porous Au nanospheres were added into a 1.5 mL centrifuge tube and ultrasonized for 30 min. Then, the drops are dried on a dry electrode and placed in the glassware of the prepared solution described above for testing.

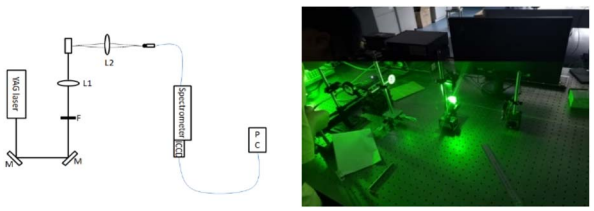

Fig. 1 Raman device diagram.

2.5 Assembly of enhanced Raman device

The Raman device of this experiment was shown in the Fig. 1, which was mainly composed of laser light source, ablation light path and signal collection light path, sampling control system, spectrum detection system and other parts.

The Q-switched YAG (indi-10) nanosecond laser with 532 nm output was used as the ablation laser source. The repetition rate is 10 Hz, the pulse width is 8 ns and the single pulse energy is more than 1.5 mJ. The output energy of the laser can be continuously adjusted by the light barrier or neutral density filter. The laser energy can be accurately measured by the laser energy meter and the single pulse energy stability is maintained within 3%. After passing through the neutral density filter F, the laser beam was converged into the liquid in the cuvette by a quartz converging lens L1 with a focal length of 100 mm. The converging lens was placed on a two-dimensional precision adjusting frame to precisely control the distance from the converging lens to the center of the cuvette.

In the direction perpendicular to the ablation laser beam, the plasma emission spectrum signal generated by laser ablation of the solution in the cuvette was imaged on the input window of the optical fiber probe through the imaging lens L2 with a focal length of 70 mm and the optical fiber output end is connected with the incident slit port of the spectrometer. The sample sampling system of this experiment was made of quartz cuvette bonded on the two-dimensional electric translation table, which can control the quartz cuvette to move at an accurate speed on the two-dimensional translation table. The translation speed is controlled by computer software. The minimum step speed of the electric translation table is 0.0025 mm s^{-1}, which ensures that each pulse laser beam is incident on different points on the target surface. Spectral detection system was mainly composed of optical fiber probe, spectrometer, ICCD and computer.

The optical fiber was used to transmit the plasma emission spectral signal to the spectrometer. The aperture of the optical fiber probe is 0.6 mm, the length of the optical fiber is 1.2 m, and the spectral response range is 200–1000 nm.

The spectrometer mainly completes the spectroscopic function of the plasma emission spectrum. The grating spectrometer was used in this experiment, with a grating constant of 1200 L mm^{-1}, a focal length of 300 mm, a resolution of 0.05 nm and a slit width of 10 m.

Enhanced charge-coupled devices are mainly used in detection spectroscopy and microscopic imaging, especially in the measurement of weak transient optical signals. The ICCD used in this experiment, with an effective pixel of 1024 × 1024, belongs to the optical fiber coupled microchannel plate image intensifier (Gen II intensifier), with a maximum shutter width of 2 ns. ICCD works in the external trigger state, which is triggered synchronously by the external trigger output of Nd:YAG laser Q-switch. The ICCD gate delay, gate width, ICCD gain, burst times and other spectrum acquisition parameters were controlled by the acquisition and analysis software in the computer.

2.6 Enhanced Raman of anhydrous ethanol

At room temperature, 5.000 mL absolute ethanol was accurately measured and immediately put into the enhanced Raman device. The Raman device was used to scan the anhydrous ethanol solution at a scanning position of 500–650 nm. The enhanced Raman data at this time was recorded by a two-dimensional translation platform for multi-position scanning. So, the average value of the enhanced Raman data was obtained. Then, 100 μL porous Au nanospheres with a concentration of 0.5 mg mL^{-1} were added every 2 min. After the reaction for 1 min, the instantaneous enhanced Raman data at this time was recorded and the average value was calculated.

The catalytic sites of ethanol oxidation by porous Au nanospheres and the appropriate catalytic measurement were determined by 11 repeated experiments.

2.7 Electrochemistry enhanced Raman of anhydrous ethanol

At room temperature, 5 mL of anhydrous ethanol was accurately measured, placed in the instrument and given a potential of −0.2 to 1 V. 0.5 mL of anhydrous ethanol was sampled for testing 10 seconds later, and 0.5 mL of anhydrous ethanol was added into the instrument. 0.4 mg of the prepared porous gold nanospheres were added into the anhydrous ethanol. 10 s later, a second sample was taken for detection, and 0.5 mL of anhydrous ethanol was also added. 75 mL 0.5 M NaOH was added to the mixture solution, and the third sampling test was conducted two minutes after the reaction. In order to avoid error, each sample is tested five times.

3. Results and discussion

3.1 Preparation and characterization of porous gold nanospheres

As shown in Fig. 2a and b, the products synthesized by chloride acid and urea were characterized by SEM and TEM, corresponding images exhibited the gold–urea complex with uniform size of 80 nm was successfully prepared. Subsequently, when the gold–urea complex was burned at 180 °C, Au nanospheres with porous structure were obtained (Fig. 2c). In addition, high-magnification TEM image in Fig. 2d clearly show that such porous Au nanospheres consist of many nanoparticles with average size of 8 nm.

The chemical properties of porous gold nanospheres were studied by X-ray photoelectron spectroscopy (XPS). As shown in Fig. 3, the Au 4f XPS spectrum of porous gold nanospheres shows two strong peaks at 84.38 eV and 88.98 eV, assigned to Au $4f_{7/2}$ and Au $4f_{5/2}$ respectively. However, the XPS spectra of unfired gold–urea complex contain Au $4f_{7/2}$, Au $4f_{5/2}$, Au^{3+} $4f_{7/2}$ and Au^{3+} $4f_{5/2}$ peaks. This result indicates that the formation of multi-empty gold nanospheres are metallic Au rather than Au^{3+}.

3.2 Catalysis of anhydrous ethanol with porous gold nanospheres

The enhanced Raman spectrum obtained by scanning the anhydrous ethanol solution was shown in Fig. 4. The abscissa wave number in Fig. 4 was obtained according to the following formula, where $\lambda_1 = 532$ nm.

$$\nu = \left(\frac{1}{\lambda_1} - \frac{1}{\lambda_2}\right) \times 10^7$$

As shown in Fig. 4, there are nine obvious Raman peaks respectively located at 888 cm^{-1}, 1054 cm^{-1}, 1102 cm^{-1}, 1283 cm^{-1}, 1458 cm^{-1}, 2884 cm^{-1}, 2928 cm^{-1} and 2976 cm^{-1}. The characteristic peak of 888 cm^{-1} is generated by the in-plane contraction of C–C–O; the characteristic bimodal C–C–O at 1054 cm^{-1} and 1102 cm^{-1} is produced by out-of-plane contraction; the characteristic peak of 1283 cm^{-1} is produced by C–O–H bending vibration; the Raman peak of 1458 cm^{-1} is caused by the asymmetric deformation of $-CH_3$; the Raman peaks of 2884 cm^{-1}, 2928 cm^{-1} and 2976 cm^{-1} are generated by the symmetric stretching vibration of $-CH_2$ and $-CH_3$, the asymmetric stretching vibration of $-CH_2$ and the asymmetric stretching vibration of $-CH_3$.[25] The Raman spectra of anhydrous ethanol at the excitation wavelength of 532 nm are basically consistent with those recorded in the literature. Therefore, subsequent results have certain credibility. Because of the surface plasmon resonance characteristics, the porous gold

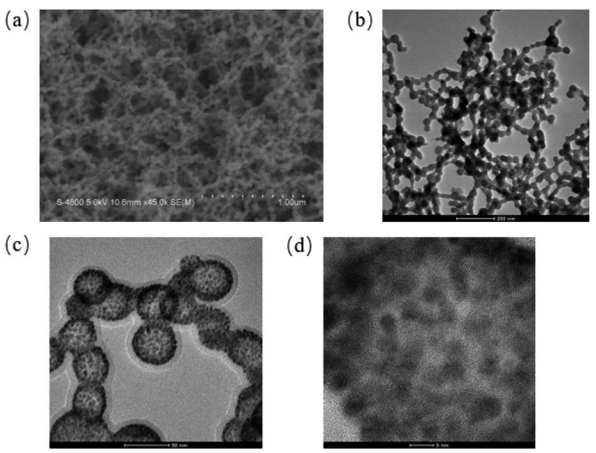

Fig. 2 SEM (a) and TEM (b) images of the gold–urea complex, low (c) and high (d) magnification TEM images of porous Au nanospheres.

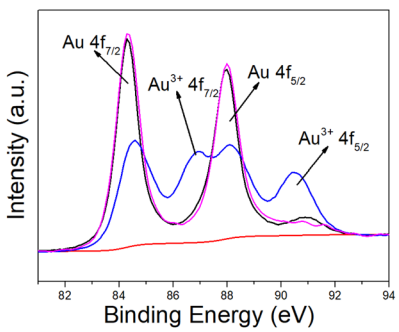

Fig. 3 Au 4f XPS spectrum of the as-prepared porous gold nanospheres.

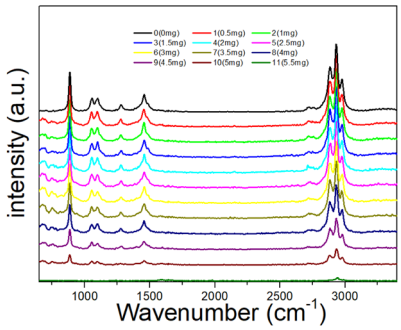

Fig. 4 Enhanced Raman spectra obtained by repeated addition of porous Au nanospheres for 10 times.

nanospheres can absorb the excitation light of the irradiated samples, which actually reduces the internal excitation light intensity of the irradiated samples and the Raman spectrum peak intensity of anhydrous ethanol. Therefore, with the increase of the amount of porous gold nanospheres, the Raman peak strength showed a decreasing trend (as shown in group 5–11 of Fig. 4). However, it is find that only when the amount of porous Au nanospheres increases to a certain extent, the characteristic Raman signal begins to decrease. When a small amount is added, the characteristic Raman signal of ethanol is gradually enhanced, especially at 2750–3000 cm^{-1} wavenumber (as shown in group 0–4 of Fig. 4).

Since the same amount of porous Au nanospheres was added each time, the peak intensity of the porous Au nanospheres is reduced by the same latitude. As shown in Fig. 5a, the peak intensity of local characteristic Raman peak increased before the third addition of porous Au nanospheres, indicating that the chemical bond interaction between porous Au nanospheres and anhydrous ethanol at this time was greater than the intensity of its absorption of excitation light. At the 3rd to 5th time, the peak intensity of the characteristic Raman peak tends to be stable, which means that the chemical bond interaction between the porous Au nanospheres and anhydrous ethanol at this time tends to be close to the intensity of its absorption of excited light. When added to 6th to 7th, the peak intensity of the local characteristic Raman peak decreases and the decline is more and more large, which indicates that the chemical bond interaction between the porous Au nanospheres and anhydrous ethanol is less than its absorption intensity of excitation light at this time.

However, when added to 8 times, the peak intensity of local characteristic Raman peak decreased significantly and the decreasing range tended to be stable. It indicates that the interaction of chemical bond between the porous Au nanospheres and anhydrous ethanol is far less than the intensity of absorption and excitation light, so the catalytic efficiency is close to saturation. Fig. 5b is a linear fitting based on the 8th to 11th Raman intensity data, which shows that the Raman intensity of these four points has a good linear relationship. Therefore, it can be concluded that when the dosage of porous Au nanospheres is 0.4 mg, the catalytic efficiency tends to be saturated. Fig. 5c is the compensated Raman peak intensity scatter diagram. It can be clearly observed in Fig. 5c that the porous Au nanospheres have a significant enhancement effect on 2930 cm^{-1} Raman peak, that is, under the action of porous Au nanospheres, the –CH_2 asymmetric stretching vibration of anhydrous ethanol is more active. Electrochemical enhanced Raman (Fig. 5d) results showed that a new peak appeared at 1379 cm^{-1} under a certain potential, which was the in-plane bending vibration of methylene C–H.

With the addition of porous gold nanospheres, the peak intensity increases. When anhydrous ethanol was catalyzed, the new peak gradually disappeared. It can be concluded that the increase of Raman peak strength after the addition of porous gold nanospheres is not caused by the Raman strength of gold, but by the interaction of chemical bonds between porous gold nanospheres and anhydrous ethanol. Therefore, under the action of porous gold nanospheres, the C–H of anhydrous ethanol will be more active and more prone to fracture. Consequently, the C–H bond of –CH_2 is more easily broken in the process of catalytic oxidation of anhydrous ethanol, which promotes the process of catalytic oxidation.

As shown in Fig. 6a, the oxidation peak appears at 0.279 V and the peak current is -3.6×10^{-5} A; the reduction peak

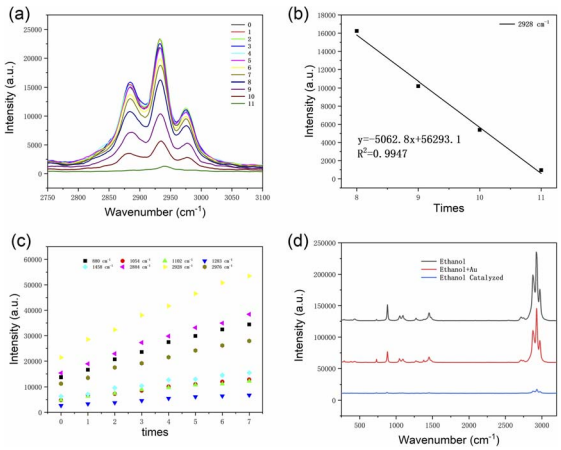

Fig. 5 (a) Local Raman spectra with a wavenumber of 2884 cm^{-1}, 2928 cm^{-1} and 2976 cm^{-1}. (b) The influence of surface plasmon resonance characteristics of porous Au nanospheres on Raman intensity. (c) Enhanced Raman intensities at various peak locations of anhydrous ethanol. (d) Electrochemical-enhanced Raman spectroscopy of ethanol.

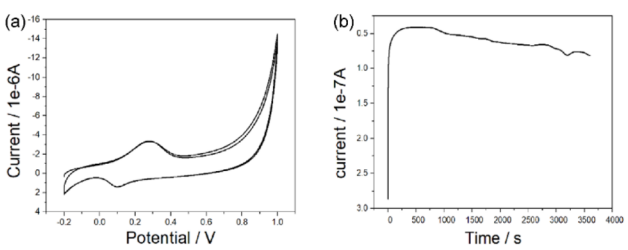

Fig. 6 (a) CV and (b) i–t curves of ethanol solution catalyzed by porous Au nanoparticles.

appears at 0.102 V and the peak current is 1.8×10^{-5} A. The effective area of the electrode is calculated according to Randles-Sevcik formula:

$$i_p = \left(2.69 \times 10^5\right) n^{\frac{3}{2}} A D^{\frac{1}{2}} v^{\frac{1}{2}} C$$

A is the effective area of the electrode, cm^2; D is the diffusion coefficient of the reactants, $cm^2\ s^{-1}$; n is the electron transfer number of the electrode reaction, v is the scanning rate V s^{-1}, C is the concentration of the reactants, mol s^{-3} and i_p is the peak current, A. Thus, the activation area of the electrode is 0.1725 cm^2. The reversibility of electrode reaction is good. In addition, as shown in Fig. 6b, when the constant potential was applied to the electrode material for a long time, the current value obtained is relatively stable, indicating that the material has good stability.

The OH^- ions in the alkaline medium adsorbed on the gold electrode and became the active center of the reaction. When the potential is less than 0.6, the ethanol molecules are adsorbed on the active center and oxidized to form CH_3CH_2O and H_2O; at the potential is more than 0.8, CH_3CH_2O was also adsorbed on the electrode and further oxidized to CH_3COOH with the formation of H_2O. In summary, in alkaline environment, the –OH group adsorbed on the electrode surface is the active center and the adsorption of –OH group on the electrode surface promotes the dissociation of C–H in ethanol-methylene, inducing the formation of water. Therefore, the porous Au nanospheres as a catalyst has good catalytic performance for the catalytic oxidation of ethanol.

4. Conclusions

In summary, enhanced Raman spectroscopy showed that the active sites of ethanol after porous Au nanospheres was $-CH_2$, which enhanced the activity of C–H in $-CH_2$. In electrochemical experiments, the active site on the electrode promotes the dissociation of C–H in ethanol-methylene to form water. Therefore, when the porous Au nanospheres are used as catalyst, the catalytic oxidation reaction of ethanol is easier to occur, and the oxidation decomposition of ethanol is accelerated, which has a better catalytic performance.

Conflicts of interest

The authors declare no competing financial interest.

Acknowledgements

This research was funded by the Overseas Visiting and Training Program for the Outstanding Young Talents in the Colleges of Anhui Province, grant number gxgwfx2018055, Anhui Provincial University Science Research projects, grant number KJ2020A0596, the Natural Science Foundation of Anhui Province, grant number 2108085QH370, and the University Synergy Innovation Program of Anhui Province, grant number GXXT-2021-013.

References

1 X. Liu, L. He, Y. Liu and Y. Cao, Supported gold catalysis: from small molecule activation to green chemical synthesis, *Acc. Chem. Res.*, 2014, **47**, 793–804.
2 Q. Zhang, B. Zang and S. Wang, Surfactant-free synthesis of porous Au by a urea complex, *RSC Adv.*, 2019, **9**, 23081–23085.
3 H. Li, J. Pan, C. Gao, M. Ma, L. Lu, Y. Xiong, *et al.*, Mercapto-Functionalized Porous Organosilica Monoliths Loaded with Gold Nanoparticles for Catalytic Application, *Molecules*, 2019, **24**, 4366–4376.
4 Y. Zhang, X. Cui, F. Shi and Y. Deng, Nano-gold catalysis in fine chemical synthesis, *Chem. Rev.*, 2012, **112**, 2467–2505.
5 C. Della Pina, E. Falletta, L. Prati and M. Rossi, Selective oxidation using gold, *Chem. Soc. Rev.*, 2008, **37**, 2077–2095.
6 X. Li, P. Li, J. Liu, *et al.*, Copper(II)-containing tungstotellurates(VI): syntheses, structures and their catalytic performances in selective oxidation of thioethers [J], *RSC Adv.*, 2020, **10**(38), 22515–22521.
7 S. Golonu, G. Pourceau, L. Quéhon, A. Wadouachi and F. Sauvage, Insight on the Contribution of Plasmons to Gold-Catalyzed Solar-Driven Selective Oxidation of Glucose under Oxygen, *Sol. RRL*, 2020, **4**, 2000084.
8 M. Liu, J. Wang, Y. Liu, R. Lu and S. Zhang, Facile Synthesis of Small Gold Nanoparticles Stabilized by Carbon Nanospheres for Selective Hydrogenation of 4-Nitrobenzaldehyde, *Bull. Korean Chem. Soc.*, 2019, **40**, 997–1001.
9 M. C. Lozano-Martín, E. Castillejos, B. Bachiller-Baeza, I. Rodríguez-Ramos and A. Guerrero-Ruiz, Selective 1,3-butadiene hydrogenation by gold nanoparticles on novel nano-carbon materials, *Catal. Today*, 2015, **249**, 117–126.
10 R. Zhang, B. Zhao, L. He, *et al.*, Cost-effective promoter-doped Cu-based bimetallic catalysts for the selective hydrogenation of C_2H_2 to C_2H_4: the effect of the promoter on selectivity and activity, *Phys. Chem. Chem. Phys.*, 2018, **20**, 17487–17496.
11 M. Bao, W. Lu, Y. Cai, L. Qiu and X. Xu, Gold(I)-Catalyzed Cyclization/Carbonylation Cascade Reaction of 1,6-Diynes: An Access to β, γ-Unsaturated Ketones, *J. Org. Chem.*, 2017, **82**, 13386–13395.
12 T. Mitsudome, A. Noujima, T. Mizugaki, K. Jitsukawa and K. Kaneda, Highly efficient double-carbonylation of amines to oxamides using gold nanoparticle catalysts, *Chem. Commun.*, 2012, **48**, 11733–11735.
13 T. Sueda, A. Kawada, Y. Urashi and N. Teno, Ag- and Au-catalyzed addition of alcohols to ynimides: β-regioselective carbonylation and production of oxazoles, *Org. Lett.*, 2013, **15**, 1560–1563.
14 S. Kumar, S. Banerjee and T. Punniyamurthy, Transition metal-catalyzed coupling of heterocyclic alkenes *via* C–H functionalization: recent trends and applications, *Org. Chem. Front.*, 2020, **7**, 1527–1569.
15 T. Sakai, C. Okumura, M. Futamura, N. Noda, A. Nagae, C. Kitamoto, *et al.*, Gold(I)-Catalyzed Cyclization-3-Aza-

Cope-Mannich Cascade and Its Application to the Synthesis of Cephalotaxine, *Org. Lett.*, 2021, **23**, 4391–4395.

16 C. Emmaniel Raju, V. Kadiyala, G. Sreenivasulu, P. Kumar, B. Sridhar and G. Karunakar, HGold-catalyzed synthesis of 1-isochromene-4-carbaldehydes oxidative cascade cyclization, *Org. Biomol. Chem.*, 2021, **19**, 3634–3643.

17 L. Bobadilla, T. Blasco and J. Odriozola, Gold(III) stabilized over ionic liquids grafted on MCM-41 for highly efficient three-component coupling reactions, *Phys. Chem. Chem. Phys.*, 2013, **15**, 16927–16934.

18 B. T. Elie, C. Levine, I. Ubarretxena-Belandia, A. Varela-Ramirez, R. J. Aguilera, R. Ovalle, *et al.*, Water Soluble Phosphane–Gold(I) Complexes. Applications as Recyclable Catalysts in a Three-component Coupling Reaction and as Antimicrobial and Anticancer Agents, *Eur. J. Inorg. Chem.*, 2009, 3421–3430.

19 L. Liu, X. Tai and X. Zhou, Au^{3+}/Au^{0} Supported on Chromium(III) Terephthalate Metal Organic Framework (MIL-101) as an Efficient Heterogeneous Catalyst for Three-Component Coupling Synthesis of Propargylamines, *Mater*, 2017, **10**, 99–110.

20 I. Savva, A. S. Kalogirou, M. Achilleos, E. Vasile, P. A. Koutentis and T. Krasia-Christoforou, Evaluation of PVP/Au Nanocomposite Fibers as Heterogeneous Catalysts in Indole Synthesis, *Molecules*, 2016, **21**, 1218–1230.

21 A. Mato, J. Agundez, C. Marquez-Alvarez, A. Mayoral and J. Perez-Pariente, Modulation of the Activity of Gold Clusters Immobilized on Functionalized Mesoporous Materials in the Oxidation of Cyclohexene *via* the Functional Group. The Case of Aminopropyl Moiety, *Molecules*, 2020, **23**, 5756–5775.

22 P. Bera, A. L. Camara, A. Hornés and A. Martínez-Arias, Comparative *in situ* DRIFTS-MS study of 12CO- and 13CO-TPR on CuO/CeO_2 catalyst, *J. Phys. Chem. C*, 2009, **113**, 10689–10695.

23 E. Groppo, A. Lazzarini, M. Carosso, A. Bugaev, M. Manzoli, R. Pellegrini, *et al.*, Dynamic Behavior of Pd/P4VP Catalyst during the Aerobic Oxidation of 2-Propanol: A Simultaneous SAXS/XAS/MS Operando Study, *ACS Catal.*, 2018, **8**, 6870–6881.

24 W. Yuan, B. Zhu, X. Y. Li, T. W. Hansen and Y. Wang, Visualizing H_2O molecules reacting at TiO_2 active sites with transmission electron microscopy, *Science*, 2020, **367**, 428–430.

25 F. Sébastien, D. Florence and C. Bertrand, Ethanol hydrates and solid solution formed by gas condensation: an *in situ* study by micro-Raman scattering and X-ray diffraction, *J. Phys. Chem. A*, 2010, **114**, 10646–10654.